Title
Gamma-ray polarization sensitivity of the gammasphere segmented germanium Detectors

Journal
Nuclear Instruments and Methods in Physics Research A, 417(1)

Author
Schmid, G.J.

Publication Date
1997-12-01

LBNL-41340
UC-413
Preprint

ERNEST ORLANDO LAWRENCE
BERKELEY NATIONAL LABORATORY

Gamma-Ray Polarization Sensitivity of the Gammasphere Segmented Germanium Detectors

G.J. Schmid, A.O. Macchiavelli, S.J. Asztalos, R.M. Clark, M.A. Deleplanque, R.M. Diamond, P. Fallon, R. Kruecken, I.Y. Lee, R.W. MacLeod, F.S. Stephens, and K. Vetter

Nuclear Science Division

December 1997

Submitted to
Nuclear Instruments and Methods in Physics Research A

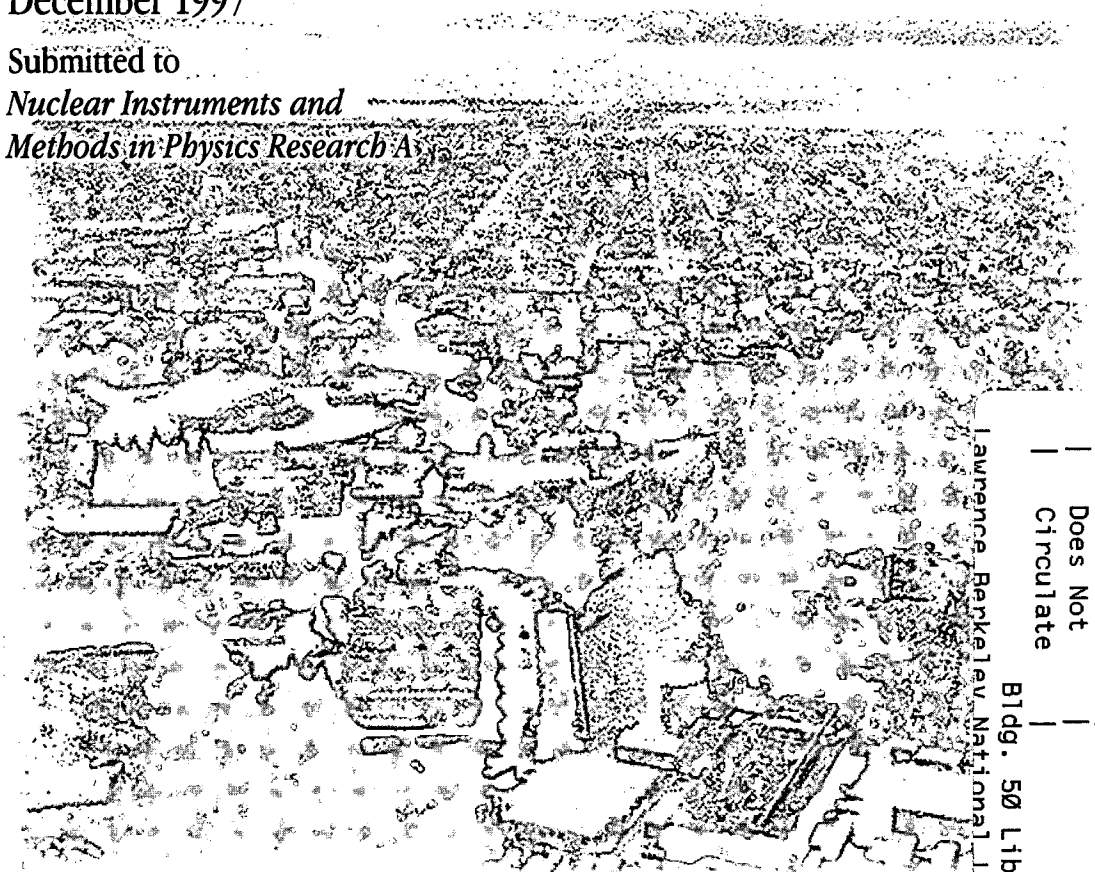

DISCLAIMER

LBNL-41340
UC-413

Gamma-Ray Polarization Sensitivity of the Gammasphere Segmented Germanium Detectors

G.J. Schmid[1], A.O. Macchiavelli, S.J. Asztalos, R.M. Clark, M.A. Deleplanque, R.M. Diamond, P. Fallon, R. Kruecken, I.Y. Lee, R.W. MacLeod,
F.S. Stephens, and K. Vetter

Nuclear Science Division
Ernest Orlando Lawrence Berkeley National Laboratory
University of California, Berkeley, California 94720 USA

[1]Isotopes Division
Lawrence Livermore National Laboratory
University of California, Livermore, California 94550 USA

December 1997

This work was supported in part by the Director, Office of Energy Research, Office of High Energy and Nuclear Physics, Division of High Energy Physics, of the U.S. Department of Energy under Contract No. DE-AC03-76SF00098.

Gamma-Ray Polarization Sensitivity of the Gammasphere Segmented Germanium Detectors

G.J. Schmid, A.O. Macchiavelli, S.J. Asztalos, R.M. Clark, M.A. Deleplanque, R.M. Diamond, P. Fallon, R. Kruecken, I.Y. Lee, R. W. MacLeod, F.S. Stephens, K. Vetter

Lawrence Berkeley National Laboratory, Berkeley, CA 94720

Abstract: We present a technique for operating the Gammasphere segmented Ge detectors as γ-ray polarimeters. Using γ rays of known polarization, we have measured the polarization sensitivity, $Q(E_\gamma)$, of these detectors in the energy range E_γ=0.4-1.4 MeV. The experimentally obtained value of Q ranges from 5% at 415 keV to 4% at 1368 keV. The magnitude and energy dependence of $Q(E_\gamma)$ has also been determined theoretically by means of a Monte Carlo simulation, and the agreement between experiment and theory is within 20% over the energy range measured. In order to investigate the potential for operating Gammasphere as a γ-ray polarimeter in a high background environment (one which is typical of high-spin nuclear structure studies), we also discuss data that we have analyzed from the ^{176}Yb(^{26}Mg,5n)^{197}Pb reaction at E=135 MeV. Although the polarimeter performance of Gammasphere is seen to be relatively poor, we are still able to demonstrate, by way of γ-ray polarization measurements, that "Shears Band 1" in ^{197}Pb should have negative parity.

PACS #'s: 24.70.+s, 29.30.kv, 29.40.-n

Keywords: Gamma-ray polarimeter, 197Pb level scheme

1. Introduction

The Gammasphere array [1], currently located at the Lawrence Berkeley National Laboratory, is a 4π γ-ray detector used primarily for accelerator-based nuclear structure studies. In the "full-implementation" mode, Gammasphere consists of 110 Compton suppressed, co-axial, Germanium detectors. In order to reduce Doppler broadening effects in the γ-ray spectrum, approximately 70% of these detectors are segmented longitudinally. It has been suggested [2] that this segmentation could also be useful as a technique for measuring the γ-ray linear polarization. In particular, since a γ ray will always Compton scatter preferentially in a direction which is perpendicular to its electric vector, the fraction of full-energy absorption events which share their energy between the two detector sides will be a function of the angle between the incident electric vector and the line of segmentation between the two sides.

In this paper, we document a series of experiments that have been done to quantify the γ-ray polarization sensitivity, $Q(E_\gamma)$, of the Gammasphere segmented Ge detectors. Data was acquired for the $^{24}Mg(p,p'\gamma)$ reaction at E_p=2.46 MeV, the $^{56}Fe(p,p'\gamma)$ reaction at E_p=3.0 MeV, and the $^{109}Ag(p,p'\gamma)$ reaction at E_p=2.54 MeV. The reactions allow determination of $Q(E_\gamma)$ at the following energies (respectively): E_γ=1368 keV, 847 keV, and 415 keV. The obtained results for $Q(E_\gamma)$ will be compared to the performance of other recently built γ-ray polarimeters [3,4,5]. In addition to this experimental work, we discuss a full Monte Carlo simulation that has been done to determine, theoretically, the magnitude and energy dependence of $Q(E_\gamma)$ for the current segmented detectors. This allows reliable extrapolation of $Q(E_\gamma)$ to energies that were not explicitly measured.

In order to demonstrate how Gammasphere can be used as a Compton polarimeter, we also discuss here an analysis of $^{176}Yb(^{26}Mg,5n)^{197}Pb$ data that was taken with Gammasphere in 1996 [6]. In this analysis, we concentrate on obtaining the sign of the γ-ray linear polarization, P, of the linking transition in ^{197}Pb between the bottom of "Band 1" and the known $I=25/2^+$ spherical state [7]. We then use this sign to deduce the

electric/magnetic (E/M) character of the transition. The results of this analysis can then be used to determine the parity of Shears Band 1. Based on a proposed configuration, a tentative assignment of negative parity has recently been made for this band [7]. The parity and configuration of Band 1 are of particular interest because its states are thought to arise from the "Shears" mechanism [8].

2. The Gammasphere Segmented Germanium Detectors

2.1 Overview of design and operation

Figure 1 shows the geometry of the Gammasphere coaxial segmented Ge detectors. The typical dimensions are as follows: diameter of 7 cm, length of 8 cm, and a co-axial hole diameter of 0.8 cm (where the co-axial hole starts at the back of the crystal and comes to within 0.8 cm of the front face). A given Gammasphere detector will vary from these average dimensions by a few percent. The segmentation of the Ge detector is accomplished by means of a segmented outer contact rather than a physical segmentation of the crystal. The signals which are read out by the associated electronics are a "full-energy" signal from the inner contact (which represents the total energy deposited on both sides of the detector), and a "side-energy" signal from one of the outer segmented contacts. The energy threshold on both the full-energy and side-energy signals is typically set at 60 keV.

Figure 2 shows a comparison between the full-energy spectrum and the side-energy spectrum as acquired using a ^{152}Eu source. The larger background of the side-energy spectrum is due to the smaller amount of Ge covered by the side-signal (i.e. the side-signal integrates only one-half of the total Ge volume), and thus the side-energy spectrum is more susceptible to Compton escapes. A very large difference in energy resolution between the full and side-energy spectra is also noticeable. The finite energy resolution of the full-energy spectrum (FWHM=Γ=2.5 KeV at 1.332 MeV) is due to the approximately equal contribution of two causes: statistics corresponding to the number of charge carriers released per γ ray; and electronic noise. The energy resolution of the side-energy

spectrum, on the other hand, is dominated by an electronic noise component which arises because the side-channel signals are taken from the outer contact of the co-axial detector, and thus significant capacitance to ground is present. Since this noise component is independent of γ-ray energy, the energy resolution of the side-energy spectrum is thus independent of energy, and has a typical value of about Γ=25 keV. Figure 3 shows the energy dependency of the energy resolution for both the full and side spectra.

2.2 Use for Doppler broadening correction

In typical heavy-ion reactions in nuclear structure studies, γ rays can be emitted while the nucleus is in flight, and this leads to a third component to the energy resolution: the width due to Doppler broadening. With this third component, the general expression for the energy resolution can then be given as follows:

$$\Gamma^2_{total} = \Gamma^2_{statistics} + \Gamma^2_{noise} + \Gamma^2_{Doppler} \tag{1}$$

The Doppler shift of a γ ray emitted by a nucleus in-flight is given by the following formula:

$$E = E_0\left(1 + \frac{v}{c}\cos\theta\right), \tag{2}$$

where E_0 is the unshifted γ-ray energy, E is the Doppler shifted γ-ray energy, v is the velocity of the recoiling nucleus in the lab frame (where we assume that v<<c), and θ is the angle of the emitted γ ray with respect to the beam direction.

Doppler broadening of spectrum peaks arise when the detector subtends a finite solid angle, and thus encounters a range of Doppler shifted energies from a given transition (since E=E(θ)). The dependence of the broadening, $|\partial E|$, on θ is obtained by taking the partial derivative of (2):

$$|\partial E| = E_0 \frac{v}{c} \sin\theta \partial\theta, \tag{3}$$

where $\partial\theta$ can be taken to represent the opening angle of the detector as seen from the target.

Equation 3 demonstrates that the Doppler broadening will be most significant at θ=90°, and that in order to minimize the broadening, the opening angle of the detector must also be minimized. This line of reasoning motivated the segmentation of all Gammasphere Ge detectors in the neighborhood of 90°. The longitudinal segmentation shown in Figure 1, when oriented in a direction perpendicular to the beam direction, allows a reduction in the detector opening angle by a factor of two, and this has allowed significant reductions of Doppler broadening, and thus significant improvements in overall detector resolution.

2.3 Use as a gamma-ray polarimeter

Although not designed with γ-ray polarization in mind, a Gammasphere segmented detector can be operated as a simple Compton polarimeter. The principle behind a Compton polarimeter is to take advantage of the polarization dependence of the Compton scattering. This polarization dependence is expressed by the Klein-Nishina formula. After summing over outgoing polarization directions, the Klein-Nishina formula takes the following form:

$$\frac{d\sigma}{d\Omega}(\theta_c, \phi_c) = \frac{1}{2} r_0^2 \frac{E_\gamma'^2}{E_\gamma^2} \left(\frac{E_\gamma'}{E_\gamma} + \frac{E_\gamma}{E_\gamma'} - 2\sin^2\theta_c \cos^2\phi_c \right), \tag{4}$$

where $d\sigma/d\Omega$ is the differential cross section, r_0 is the classical electron radius, E_γ is the energy of the incident γ ray, E'_γ is the energy of the Compton scattered γ ray, θ_c is the polar Compton scattering angle, and ϕ_c is the azimuthal scattering angle (the angle between

the electric vector of the incident γ ray and the plane containing the incident and scattered γ ray).

Using conservation of energy and momentum for the Compton scattering process, we can relate E_γ and E'_γ in the following manner:

$$E'_\gamma = \frac{0.511}{1 + \frac{0.511}{E_\gamma} - \cos\theta_c}, \tag{5}$$

where E_γ and E'_γ are in MeV

It can be noticed that the Klein-Nishina formula shows a clear preference for scattering into azimuthal directions which are perpendicular to the incident electric vector (i.e. $d\sigma/d\Omega$ is maximum for ϕ_c=90°). By measuring an asymmetry between up-down and left-right azimuthal scattering for an incident γ-ray beam, one can hope to determine its polarization. An ideal design for a polarimeter, therefore, would consist of 5 elements lying in a plane perpendicular to the beam direction: a central scatterer, and four "analyzing" detectors located at ϕ=0° (up), 90°(right), 180° (down), and 270° (left) with respect to the scatterer. Such a design was used in the "POLALI" polarimeter of [5]. This number of 5 total elements can easily be reduced to 4 because one of the analyzers can also serve as the scatterer. This yields the popular four-fold segmented design which has been the basis for several recent polarimeters ([3,4] and the "MINIPOLA" in [5]).

A two-fold segmented design, such as the one shown in Figure 1, can also be used as a polarimeter by defining two experimental quantities of interest: the number of detector photopeak events which confine themselves completely to either one side or the other (the "confined" events); and the number of photopeak events that share the energy between the two sides (the "shared" events). Figure 4 shows the situation whereby a γ ray with its electric vector parallel to the line of segmentation is incident on the detector. Left-Right scattering (most probable in this case) will likely give a shared event. Up-down scattering

with the geometry of Figure 4 is more likely to give a confined event. The confined and shared events can then be used to calculate an experimental "asymmetry" which is analogous to the asymmetry of the four-fold segmented detector. This asymmetry can then be used to determine the γ-ray polarization. More details on this procedure appear in the next section.

3. Gamma-ray Polarization Formalism

3.1 Introduction

For a general review of the formalism of γ-ray polarization and γ-ray polarimeters, the reader is referred to the paper by Fagg and Hanna [9]. From [9], we get the standard definition of γ-ray linear polarization, P(θ), which is appropriate for nuclear reaction studies:

$$P(\theta) = \frac{J_0 - J_{90}}{J_0 + J_{90}}, \tag{6}$$

where J_0 is the average component intensity of the γ-ray electric vector in the reaction plane (the plane containing the incident particle beam and the outgoing γ ray), J_{90} is the intensity perpendicular to this plane, and θ is the angle of the polarimeter with respect to the incident beam direction.

Using the angular correlation formalism presented in [9], we can re-cast (6) into the following form:

$$P(\theta) = \frac{\sum_{\nu} a_\nu \kappa(LL')P_\nu^2(\cos\theta)}{1 + \sum_{\nu} a_\nu P_\nu(\cos\theta)}, \tag{7}$$

where the a_ν coefficients are the normalized Legendre coefficients; the $P_\nu(\cos\theta)$ are the ordinary Legendre polynomials; the $P_\nu^2(\cos\theta)$ are the associated Legendre polynomials;

and the $\kappa(LL')$ are quantities which depend on the multipolarities which are present (L,L'), and have their values given in [9]. Equation 7 is required when one wants to extract $P(\theta)$ from an angular distribution measurement that has been fitted to Legendre polynomials.

3.2 Traditional formalism

Here we present the formalism that is associated with the recent four-fold segmented polarimeters of [3,4,5], and also with many of the polarimeters that have been developed during the past 30 years (e.g. [10,11,12,13]). Section 3.3, which follows, contains the new definitions that are necessary to accommodate the different situation of the two-fold segmented detector.

When one measures an experimental asymmetry from a polarimeter, it is desirable that the result be directly proportional to $P(\theta)$. In particular, we want that:

$$A(\theta) = Q(E_\gamma)P(\theta), \tag{8}$$

where the proportionality constant, $Q(E_\gamma)$, is the polarization sensitivity of the detector.

For a detector where up-down/left-right scattering asymmetries can be measured, the following formula for $A(\theta)$ is typically employed:

$$A(\theta) = \frac{N_V(\theta) - N_H(\theta)}{N_V(\theta) + N_H(\theta)}, \tag{9}$$

where N_V represents the number of vertical coincidences (i.e. up-down Compton scattering perpendicular to the reaction plane) and N_H the number of horizontal coincidences (i.e. left-right Compton scattering in the reaction plane).

If efficiency were not an issue, the ideal polarimeter would consist of 5 point detectors: one central scatterer and four surrounding analyzers. If all these detectors were to lie in a plane perpendicular to the incident γ-ray direction, and if the azimuthal angle

between the analyzers were 90 degrees, it could then be shown, using (4),(5),(8) and (9) that:

$$Q_p(E_\gamma) = \left(\frac{1}{\frac{E_\gamma}{0.511} + \frac{0.511}{E_\gamma + 0.511}} \right), \tag{10}$$

where $Q_p(E_\gamma)$ is the polarization sensitivity for point detector geometry. Finite geometry effects alter this energy dependence somewhat. However, it turns out that (10) often gives a fairly good approximation to the energy dependence of most Compton polarimeters (e.g. see discussion in [4]).

When one utilizes a polarimeter to make a γ-ray polarization measurement, the primary objective is to minimize the error in P. Using (8) and (9), one can show that the error in P, ΔP, is related to Q as follows:

$$(\Delta P)^2 = \frac{1}{N_i Q^2 \varepsilon_c}, \tag{11}$$

where N_i is the total number of incident γ-rays and ε_c is the coincidence efficiency (i.e. the probability that an incident γ ray registers a hit in both the scatterer and one of the analyzers).

For a given number of incident γ rays, is has become standard to identify $Q^2\varepsilon_c$, from (11), as a "figure of merit" (F) to be maximized. Thus we have our final equation of interest:

$$F = Q^2 \varepsilon_c. \tag{12}$$

Based on a given counting time, F can be used to compare the relative performance of different polarimeters.

3.3 New Definitions

For purpose of comparison with other standard polarimeters, we would like the Gammasphere segmented detectors to obey (8) and (12). However, the two-fold segmented nature of the current geometry renders it impossible to measure a true up-down/left-right scattering asymmetry, and thus (9) cannot be used for $A(\theta)$. While a 90 degree rotation of the segmented Ge detectors about their axes would, in fact, allow such an up-down/left-right asymmetry to be measured, such rotations are not possible given the physical structure of the Gammasphere array.

In order to deduce a new form for $A(\theta)$ which is appropriate for non-rotatable bi-segmented Ge detectors, we introduce the following definitions:

C_0,S_0 = # of confined and shared events corresponding to an incident γ-ray beam in the pure J_0 state. (13)

C_{90},S_{90} = # of confined and shared events corresponding to an incident γ-ray beam in the pure J_{90} state.

C_u,S_u = # of confined and shared events corresponding to the case of unpolarized incident γ-radiation.

C,S = # of confined and shared events corresponding to an incident γ-ray beam of arbitrary polarization.

From these definitions, the following expressions are seen to be valid:

$$C_u = \frac{1}{2}(C_0+C_{90}), \qquad S_u = \frac{1}{2}(S_0+S_{90}), \qquad C_0+S_0=C_{90}+S_{90}=\varepsilon N, \tag{14}$$

where ε is the detector photopeak efficiency and N is the total number of γ-rays emitted from the source. The third expression is understood in the light of the cylindrical

symmetry of the co-axial Ge detector. Independent of the orientation of the line of segmentation, the total number of counts detected, εN, should be constant.

For the case of arbitrary polarization, the following expressions are then seen to hold:

$$C = J_0C_0 + J_{90}C_{90}, \qquad S = J_0S_0 + J_{90}S_{90} \tag{15}$$

A natural guess for the form of A(θ) would be (C-S)/(C+S). However, it can be shown using (14) and (15) that this form is not factorable into the form of (8). Instead, we propose the following form for A(θ):

$$A(\theta) = \frac{1}{\sqrt{\eta}}\left(\frac{\eta C(\theta) - S(\theta)}{C(\theta) + S(\theta)}\right), \tag{16}$$

where $\eta = S_u/C_u$, and can (for example) be measured using an unpolarized radioactive source. Using (14) and (15), we can show that (16) is factorable into the form which we desire:

$$A(\theta) = \frac{1}{\sqrt{\eta}}\left(\frac{C_0 - C_{90}}{C_0 + C_{90}}\right)\left(\frac{J_0(\theta) - J_{90}(\theta)}{J_0(\theta) + J_{90}(\theta)}\right) = Q(E_\gamma)P(\theta). \tag{17}$$

Furthermore, if we assume that $\eta C \approx S$, and thus that $C+S \approx C(\eta+1) = N_p = \varepsilon N_i$ (where N_p is the total number of detector photopeak events, ε is the photopeak efficiency, and N_i is the number of incident γ rays) we can show that (16) yields the following form for the error in P(θ):

$$\Delta P = \frac{\Delta A}{Q} = \frac{1}{\sqrt{N_i}}\sqrt{\frac{1}{Q^2\varepsilon}}, \tag{18}$$

where we again recover, in the denominator, the desired "figure of merit", $F=Q^2\varepsilon$ (except that this time, ε is the photopeak efficiency rather than the coincidence efficiency). This recovery of the standard form for F is due to the $1/\sqrt{\eta}$ factor which we have included in (16).

4. Measurements of $Q(E_\gamma)$

4.1 Overview

The procedure used in the measurement of $Q(E_\gamma)$ is similar to that of [4]. Using γ rays of known polarization, asymmetries were measured in the Gammasphere segmented detectors and $Q(E_\gamma)$ was then determined using (8). In particular, data was acquired for the $^{24}Mg(p,p'\gamma)$ reaction at E_p=2.46 MeV, the $^{56}Fe(p,p'\gamma)$ reaction at E_p=3.0 MeV, and the $^{109}Ag(p,p'\gamma)$ reaction at E_p=2.54 MeV. The proton beams were provided by the 88" Cyclotron at the Lawrence Berkeley National Laboratory. For each reaction, the incident beam energy was chosen so as to strongly populate one of the first excited states in the target nucleus. The de-exciting γ rays, at E_γ=1368 keV in ^{24}Mg, 847 keV in ^{56}Fe, and 415 keV in ^{109}Ag, are all known to be pure E2 in nature. By measuring the angular distribution associated with each transition (by means of the Gammasphere array), the substate populations of the excited state can be obtained, and the γ-ray polarization determined. This information, combined with the asymmetries measured from the segmented detectors, allowed the determination of $Q(E_\gamma)$.

4.2 Angular distributions

The spectra acquired for the calibration reactions were exceptionally clean. The full-energy spectrum for $^{24}Mg(p,p'\gamma)$ is shown in Figure 5. The acquired angular distributions for each of the reactions are shown in Figure 6. The solid line is a Legendre polynomial fit to the data. Since the transitions are all known to be pure E2, we can then use the acquired a_2 and a_4 coefficients in (8) to get the expected $P(\theta)$ distribution. These

$P(\theta)$ distributions are shown in Figure 7. Because the polarization is strongest at 90°, the analysis with the segmented detectors has concentrated on this angle. Table I lists, for each reaction, the γ-ray energy, the a_2 and a_4 coefficients, and the predicted P(90°).

4.3 Segmented detector asymmetries

For each experiment, side-energy spectra were acquired for both the in-beam reaction of interest (e.g. $^{24}Mg(p,p'\gamma)$) and also for a ^{152}Eu source, which serves as a source of unpolarized γ rays from 100-1400 keV. To calculate A(90°) via (16), we then use the confined and shared from the in-beam experiment as C and S, and we use the ^{152}Eu data to calculate a variety of $\eta(E_\gamma)$ values. Since the energies afforded by the ^{152}Eu source do not (in general) correspond exactly to the desired γ-ray energy of the in-beam experiment, we need a procedure for obtaining a suitable value of η. If the desired energy lies close to a ^{152}Eu line, simple linear interpolation is valid. Otherwise, a spline fit, or theoretical energy dependence is needed (see section 5). With regards to the determination of η, experience has shown that it is crucial to acquire the polarized and unpolarized data as simultaneously as is possible (i.e. within a day or two of each other). If the interim between measurements is long, thresholds can change, calibrations can drift, resolutions can degrade, and, as a result, inaccurate polarization measurements can occur.

In the current series of calibration measurements, side-energy spectra were created for the segmented detectors at 90° by gating on the peak of interest in the full-energy spectrum. As an example, the side-channel spectrum for $^{24}Mg(p,p'\gamma)$ is shown in Figure 8. The confined and shared events were defined from this spectrum as follows: all side-channel events within 2 FWHM of the peak are considered confined to one side; all events from this point down to just above the zero channel are considered shared; and all events in the zero channel (where we have a count in the full-energy spectrum but have no side-channel correspondence) are considered confined to the other side. The two confined totals are then summed together to produce one overall confined figure. Due to the fact that the

FWHM in the side-energy spectrum is independent of energy, this technique for determining confined and shared is applicable to γ rays of all energies.

Having acquired confined and shared events for each transition of interest, we can then use (16) to determine A(90°) and (8) to determine $Q(E_\gamma)$ (making use of the P(90°) values from the angular distribution measurements). The results are shown in Table I.

4.4 Comparison of results to other polarimeters

Using the traditional "figure of merit", $F=Q^2\varepsilon$, we can obtain a rough comparison between the current two-fold segmented design and previous four-fold segmented designs (where $\varepsilon=\varepsilon_c$). For the 1368 keV line, Table II shows the comparison of Q, ε, and F for the polarimeter of Schlitt et al. [3], the POLALI polarimeter of [5], the MINIPOLA of [5], and the current polarimeter. This comparison would indicate that the current design is competitive with those of [3,5] (the results in [4] do not include an absolute determination of F). In particular, it is seen that the gain in ε over ε_c more than compensates for the lower Q of the current polarimeter. In an array with many detectors, such as Gammasphere, the "figure of merit" takes on the form: $F=N_dQ^2\varepsilon$, where N_d is the number of detectors involved in the measurement. With 77 segmented detectors, Gammasphere can potentially be very powerful in this respect.

In practice, however, comparisons using F are not always valid. It often turns out to be more important to obtain a clean spectrum than to obtain a spectrum with a lot of counts (e.g. if the count rate is very high, the counting time is no longer a limiting factor). In this case, Q (which is directly proportional to the measured asymmetry) is the important quantity. In this regard, the current polarimeter, with its relatively low Q, is not seen to be competitive with other recent polarimeters.

5. Monte Carlo Simulation

5.1 Overview

In order to extrapolate $Q(E_\gamma)$ to energy regions where data was not acquired, experimenters typically fit their data to a theoretical energy dependence. For standard four-fold segmented detectors, it has been empirically found that $Q_p(E_\gamma)$, the polarization sensitivity for "point-detector" geometry, is often an adequate energy dependence. However, the current data, due to the different two-fold geometry, is not well fit by this form. With this motivation, a theoretical effort was pursued to calculate $Q(E_\gamma)$ for the current geometry by means of a Monte Carlo simulation. Since commercially available codes could not be found which incorporated γ-ray polarization effects, a completely new program was written. The basic idea of this new code was to model the source-detector geometry in an exact fashion, and then simulate the multiple Compton scattering of the incident γ rays inside the Ge crystal (for the geometry in question, each 1 MeV γ ray Compton scatters ~5 times before photoabsorption). Although similar in many ways to standard Monte Carlo treatments, the novel aspect of this code was the rigorous handling of the γ-ray polarization effects in the multiple scattering. This was accomplished by taking the analytical approach derived by Wightman [14] and applying it to the Monte Carlo method. Full details of this program will be discussed elsewhere [15], but we present some of the results below.

5.2 Results of simulation for unpolarized observables

In order to test the validity of the Monte Carlo simulation discussed above, a calculation of the segmented Ge detector efficiency (for the full-energy signal) was undertaken. The calculation involved a single detector at 25 cm from a 1.332 MeV γ-ray source (on-axis). The result predicted that the photopeak efficiency should be 78% as compared with a 3"x3" NaI(Tl) detector at the same distance. The statistical error in this calculation was better than 1%. An experimental determination of the photopeak efficiency,

obtained by taking an average of the measurements for many detectors, gave 74%. This is within 5% of the calculated value.

Another unpolarized quantity that is of interest (and, furthermore, that is needed for experimental determination of A and Q) is $\eta(E_\gamma)$. If a $Q(E_\gamma)$ measurement is desired where no $\eta(E_\gamma)$ data exists, a theoretical prediction for $\eta(E_\gamma)$ can be used. Figure 9 shows the $\eta(E_\gamma)$ data acquired using a side-energy threshold of 130 keV. These data are derived from the strong lines measured using a ^{152}Eu source. For comparison, Monte Carlo simulations for $\eta(E_\gamma)$ were done at each γ-ray energy in ^{152}Eu (a few extra energies were also added). These calculations were not normalized to the data in any way. The agreement between the data and the Monte Carlo simulation is excellent.

5.3 Results of simulation for $Q(E_\gamma)$

Figure 10 shows the result of the Monte Carlo simulation for $Q(E_\gamma)$ as compared with the measured data. The agreement is within 20% over the energy region measured. The "turn over" of the curve at lower energies is especially noticeable. This facet of the energy dependence is to be expected due to the decreased mean free path for the γ rays at the lower energies. In particular, if the γ rays cannot reach the other side of the detector by one, or several, scatterings, virtually all events will be confined, and $Q(E_\gamma)$ will be very low.

If we make the assumption that the discrepancy between theory and data is due to uncertainties in the Ge detector geometry (e.g. crystal dimensions, dead layers, etc.), we can make a first order correction by simply multiplying the theoretical curve by an overall multiplicative constant so as to normalize it to the data. We can accomplish this by minimizing a χ^2 function. The resulting curve is shown in Figure 11. Using this curve, we can now obtain a reasonable estimate for Q at all energies.

6. Gamma-ray polarization measurement in ^{197}Pb

6.1 The experiment

To illustrate the technique that we have developed for γ-ray polarization measurements, we discuss here some γ ray data that we have analyzed from the ^{176}Yb(^{26}Mg,5n)^{197}Pb reaction at E=135 MeV. The beam was provided by the 88" Cyclotron at the Lawrence Berkeley National Laboratory. The ^{176}Yb target was thick enough to completely stop the ^{197}Pb recoils, and thus (due to the relatively long lifetimes of the γ-ray transitions) Doppler broadening in the γ-ray spectrum was not an issue. The segmented Ge detectors that we looked at were the 12 detectors located between 80 and 100 degrees (with respect to the beam axis). These detectors were gain matched (both full-energy and side-energy channels), and had their side-energy thresholds all set at 60 keV. During data acquisition, the confined and shared events for each detector were summed to produce a single confined and shared value for each γ-ray transition of interest.

The specific goal of this analysis was to experimentally determine the parity of Band-1 in ^{197}Pb. This band is thought to arise from the "Shears" mechanism [7], a new concept in nuclear structure physics. Figure 12 shows the most recent level scheme proposed for this nucleus [7]. A determination of E1 character for the 432 keV linking transition at the bottom of the band would verify the tentatively assigned negative parity shown in Figure 12. Since photons of electric character should have their electric vectors in the reaction plane (as defined by the beam axis and the γ-ray direction), and since the line of segmentation of the Ge detectors is always perpendicular to the reaction plane, we expect to measure a positive asymmetry (A), and therefore a positive polarization, for an E1 transition. On the other hand, the in-band transitions of band-1 are thought to be primarily M1 in character due to the nature of the Shears mechanism. For these transitions we would expect to measure a negative asymmetry, and therefore a negative polarization.

6.2 Expected magnitude of polarization for the in-band and linking transitions

Using tables of angular distribution functions for maximum possible alignment (e.g. [16]), along with equation (7), one can show that the maximum polarization for pure dipole transitions at high (half-integer) spin is 36%. Using A=PQ at 400 keV (where Q~5%), we see that we must look for experimental asymmetries which are at most 2%, and perhaps as low as 1% (when one accounts for the effects of incomplete alignment).

Recasting the form of equation (16), we obtain:

$$A(\theta) = \frac{1}{\sqrt{\eta}} \left(\frac{\eta \frac{C(\theta)}{S(\theta)} - 1}{\frac{C(\theta)}{S(\theta)} + 1} \right). \tag{19}$$

From (19), we see that it is not the absolute confined and shared peak areas that we are after, but rather the confined-to-shared yield ratio. In this manner, we can hope that systematic effects in the peak fitting procedure will cancel out to some extent.

6.3 Polarization Results

Figure 13 shows an acquired spectra for Band-1 before and after gating on the 270 keV in-band transition. The gated spectra (both confined and shared) were then analyzed to obtain the peak areas, and thus the experimental asymmetries and measured polarizations, for the following transitions: 353 keV, 294 keV, 365 keV, 385 keV, 370 keV, 359 keV (all in-band), and also the 432 keV linking transition. The peak areas were obtained by way of a peak fitting program (DAMM from Oak Ridge National Laboratory) which allowed simultaneous fitting of multiple peaks and background. The number of peaks included per fit was kept to a minimum consistent with the requirement that a good χ^2 per degree of freedom be obtained (for a small fitting region, a constant peak width vs. energy was assumed). The final results for the γ-ray polarization are shown in Figure 14. The

432 keV linking transition appears strongly positive, consistent with an assumption of E1 character. In contrast, the in-band transitions appear negative, consistent with the assumption of M1 character. These results support the assumption of negative parity for Band-1 in ^{197}Pb, and are in agreement with the polarization results from Eurogam [17].

The fact that sóme of the transitions show unrealistically high polarization magnitudes (>36%), and the fact that the in-band transitions show significant scatter about an average value, suggests that accurate polarization measurements using Gammasphere may not be possible in the high spin regime. This is most likely due to the high ambient background which limits the accuracy to which one can fit peak areas.

Alternatively, one might argue that rather than fluctuating about an average value, the polarization magnitudes in Figure 14 are actually decreasing as we move down the band. In particular, based on the irregular nature of this band (Figure 15 shows the large backbend that occurs in this region), one could perhaps speculate that the fall in polarization magnitude is due to a changing M1/E2 in-band ratio. However, this seems unlikely based on the measured angular distribution plots presented in Figure 16. In these graphs, the distributions are seen to be unchanging as one moves down the band. Based on fits to Legendre polynomials, an E2/M1 mixing ratio can be extracted by using the formalism of [16] to relate the measured a_k coefficients to the mixing ratio associated with maximum possible alignment. In this manner, we find a constant mixing ratio of ~10% for all the transitions. Therefore, rather than being due to a changing E2/M1 ratio, the apparent fall in polarization magnitude is most likely just due to systematic errors in the peak fitting procedure.

Since the γ-ray background for high-spin studies is typically quite high, and since the currently studied band is strong in comparison with other high spin bands (e.g. the other Shears bands in the Pb isotopes), it is not clear to what extent Gammasphere can be useful as a general polarimeter in the high spin regime. Acquiring adequate statistics for double or triple gating would be one possible technique for further cleaning up the spectra,

and thus improving the performance of Gammasphere polarimetry. Another possible step to improve performance would be to alter the Gammasphere support structure so as to allow rotation of each segmented Ge detector about its axis. This would make it possible to measure an up-down/left-right scattering asymmetry with a given detector (via a 90 degree rotation), and would thus eliminate the need for the $\eta(E_\gamma)$ parameter. This would help reduce possible sources of systematic error.

7. Conclusion

Although Gammasphere was not originally designed to function as a γ-ray polarimeter, we have investigated here its potential to operate as such. In particular, we have measured the γ-ray polarization sensitivity, $Q(E_\gamma)$, for the Gammasphere segmented Ge detectors over a range of energies. We have then applied this knowledge to a direct measurement of γ-ray polarizations in ^{197}Pb.

The spread of the in-band polarization data shown in Figure 14 indicates that the segmented Ge detectors are not able to operate as sensitive polarimeters in a high background environment. This problem is directly related to the low polarization sensitivity (Q) of the current two-fold segmented geometry. However, it would appear that with a careful measurement, one can still hope to differentiate between electric and magnetic transitions in the spectrum. The current γ-ray polarization study that we have done in ^{197}Pb demonstrates a different sign in γ-ray polarization between the proposed M1 transitions and the proposed E1 transition. This evidence supports the contention [7,17] that Shears Band-1 in ^{197}Pb has negative parity.

The authors would like to thank the staff of the 88" Cyclotron at Berkeley for their support. In addition, the authors would like to thank Dr. Dave Ward for helpful discussions. This work was supported by the US Dept. of Energy under contract # DE-AC03-76SF00098.

References:

1. I.Y. Lee, Nucl. Phys. **A520** (1990) 641c
2. A.O. Macchiavelli et al., *Conf. on Phys. from Large Gamma-ray Det. arrays*, Proceedings, Vol.2, p. 149, Lawrence Berkeley Laboratory, 1994
3. B. Schlitt, U. Maier, H. Friedrichs, S. Albers, et al., NIM **A337** (1994) 416
4. P.M. Jones, L.Wei, F.A. Beck, P.A. Butler, et al., NIM **A362** (1995) 556
5. A. von der Werth, F. Becker, J. Eberth, et. al. NIM **A357** (1995) 458
6. R.M. Clark et al., To be published
7. G. Baldsiefen, S. Chmel, H. Hubel, et al., Nucl. Phys. A**587**(1995)562
8. G. Baldsiefen, H. Hubel, W. Korten, et al., Nucl. Phys. A**547**(1994)521
9. L.W. Fagg, S.S. Hanna, Rev. Mod. Phys **31** (1959) 711
10. A.E. Litherland, G.T. Ewan, S.T. Lam, Can. Journ. Phys. **48** (1970) 2320
11. P.A. Butler, P.E. Carr, L.L. Gadeken, A.N. James, et al. NIM **108** (1973) 497
12. R. Bass, S. Brinkmann, C von Charzewski, H. Hanle, NIM **104** (1972) 33
13. J. Simpson, P.A. Butler, L.P. Ekstrom, NIM **204** (1983) 463
14. A. Wightman, Phys. Rev. **74** (1948) 1813
15. G.J. Schmid, et al., To be published
16. E. Der Mateosian, A.W. Sunyar, Atomic Data and Nucl. Data Tables, Vol. **13**, Num. 5, (392) 1974
17. H. Hubel, Private Communication

Figure captions:

1. The co-axial segmented Ge detectors which comprise ~70% of the Gammasphere array. The outer contact is segmented longitudinally to create two side-energy channels. The inner contact and one of the outer contacts are integrated to give the "full-energy" and "side-energy" signals respectively.
2. The ^{152}Eu spectra created by integrating the non-segmented inner contact (solid line) and one of the segmented outer contacts (dotted line).
3. The energy resolution of the full-energy channel (top) and side-energy channel (bottom) as determined from a ^{152}Eu source. The solid line represents a linear fit to the data (accomplished via χ^2 minimization).
4. The front face of a segmented Ge detector showing the co-axial hole and the effective line of segmentation. Incident γ rays will scatter preferentially in a direction which is perpendicular to their electric vector. Events whereby the deposited energy is shared between the two sides is call "Shared". Events which confine their energy entirely to one side or the other are called "Confined".
5. The "full-energy" spectrum, as integrated from the inner contact, for the ^{24}Mg(p,p'γ) experiment. The 1368 keV line is the $2^+ \rightarrow 0^+$ transition of interest.
6. Angular distributions for the (p,p'γ) reactions studied. In each case, the γ ray of interest is the transition from one of the first excited states to the ground state of the target nucleus.
7. The expected γ-ray polarizations as a function of angle for the three calibration reactions. These curves are calculated from the angular distributions in Figure 6, taking into account the known E2 character of the transitions.
8. A side-energy spectrum for ^{24}Mg(p,p'γ) which has been gated on the 1368 keV line

in the full-energy spectrum. The strong peak in this spectrum at 1368 keV represents events confined to one side, while the zeros represent events confined to the other.

9. A graph of the $\eta(E_\gamma)$ parameter, showing both experiment (solid points) and theory (open points connected by straight lines).

10. A graph of the polarization sensitivity, $Q(E_\gamma)$, showing both experiment (solid points) and theory (open points connected by straight lines). The energy threshold for the side-channel is 60 keV

11. The $Q(E_\gamma)$ curve normalized to the experimental data by means of an overall multiplicative constant.

12. The most recent level scheme for ^{197}Pb as presented in [7].

13. Confined spectra from the ^{176}Yb(^{26}Mg,5n)^{197}Pb reaction at E=135 MeV. These spectra are generated from the 12 segmented Ge detectors between 80 and 100 degrees. The top spectrum is ungated, while the bottom spectrum is gated on the 270 keV in-band transition.

14. The current results for the γ-ray polarization, P, of the in-band transitions (solid points) and the 432 keV linking transition (open point).

15. Spin vs. energy plot for Band-1 showing the large backbend.

16. Angular distributions for the ^{197}Pb transitions in the neighborhood of the backbend. The solid line is a Legendre fit including the a_2 and a_4 coefficients.

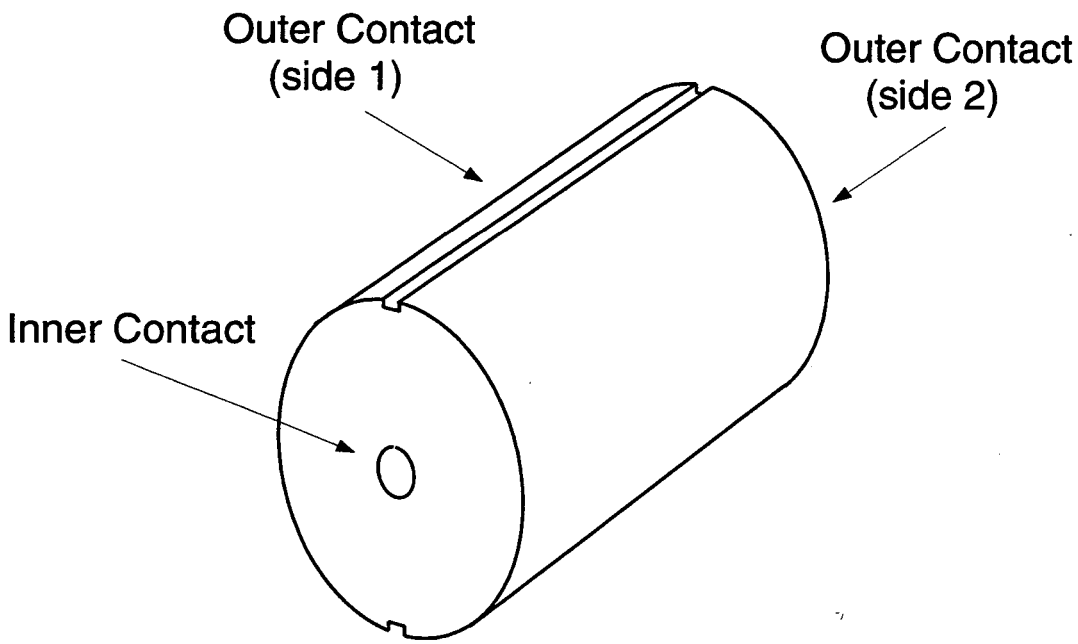

Fig. 1

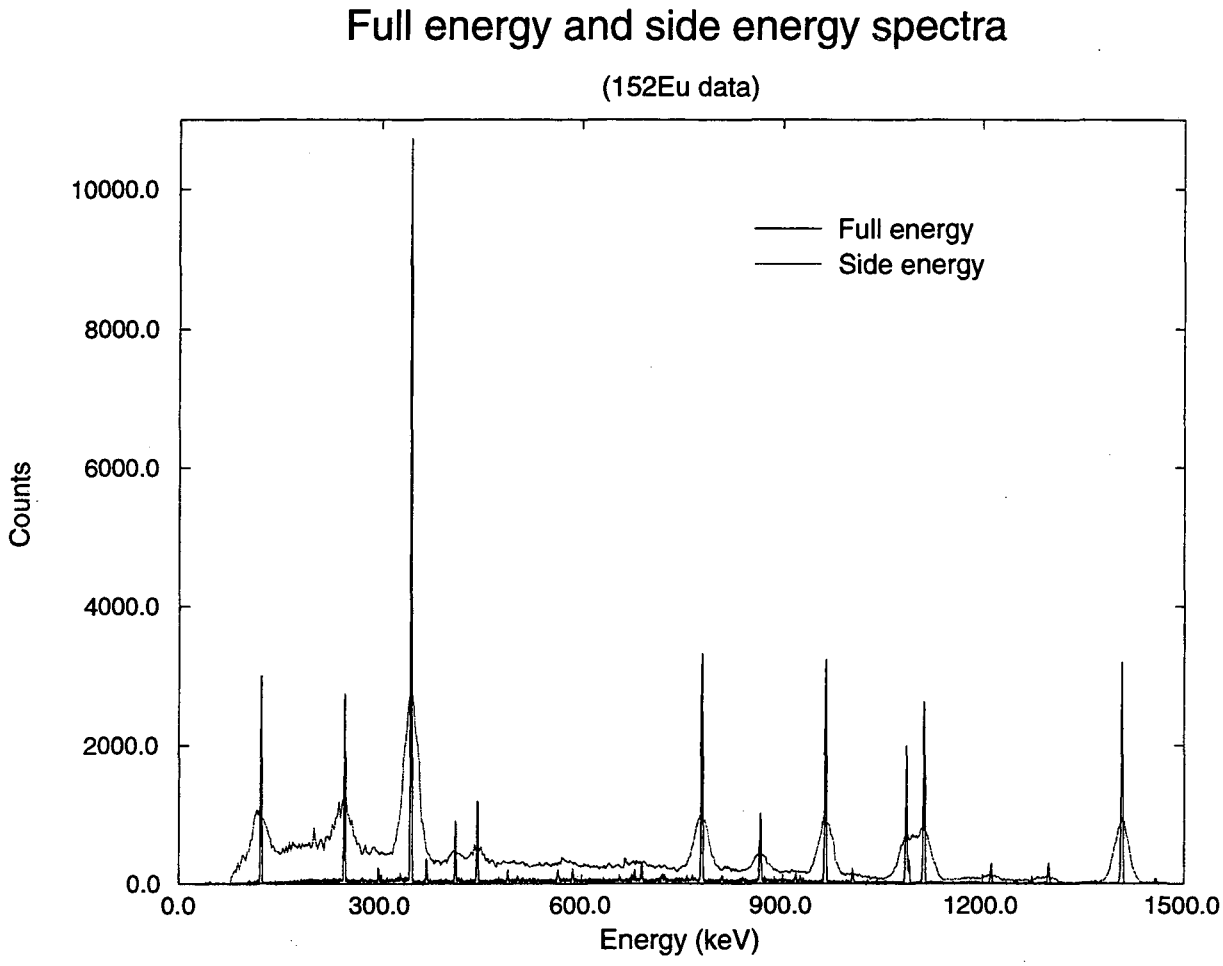
Full energy and side energy spectra
(152Eu data)
Full energy
Side energy
Counts
10000.0
8000.0
6000.0
4000.0
2000.0
0.0
0.0
300.0
600.0
900.0
1200.0
1500.0
Energy (keV)

Fig. 2

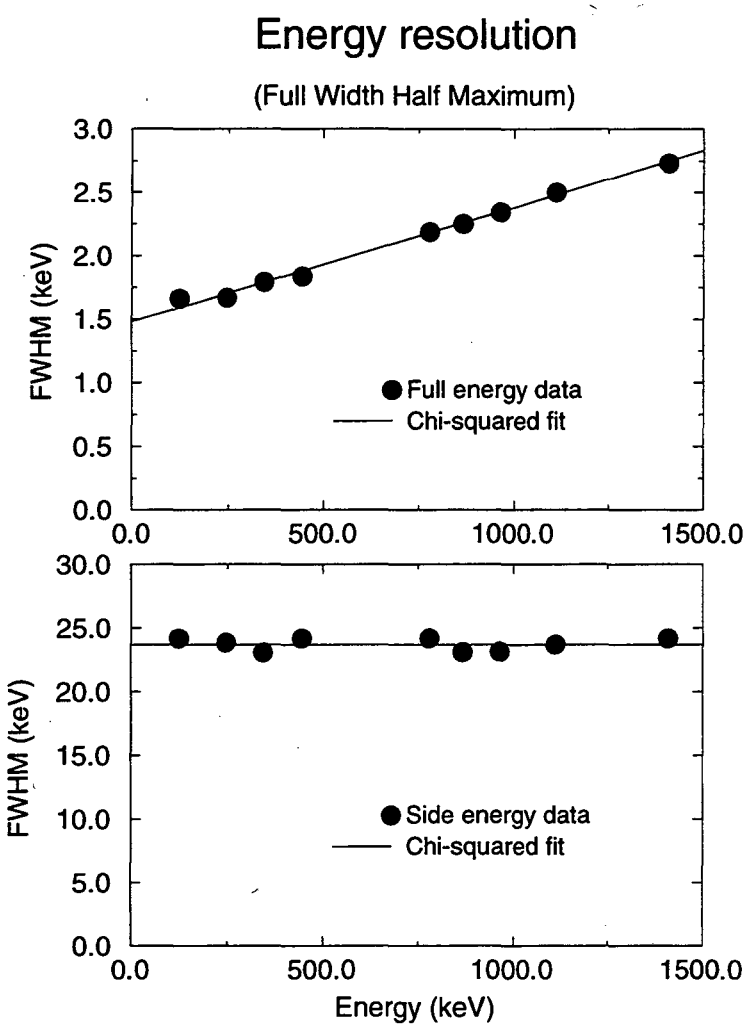
Energy resolution
(Full Width Half Maximum)
FWHM (keV)
3.0
2.5
2.0
1.5
1.0
0.5
0.0
0.0
500.0
1000.0
1500.0
Full energy data
Chi-squared fit
FWHM (keV)
30.0
25.0
20.0
15.0
10.0
5.0
0.0
0.0
500.0
1000.0
1500.0
Side energy data
Chi-squared fit
Energy (keV)

Fig. 3

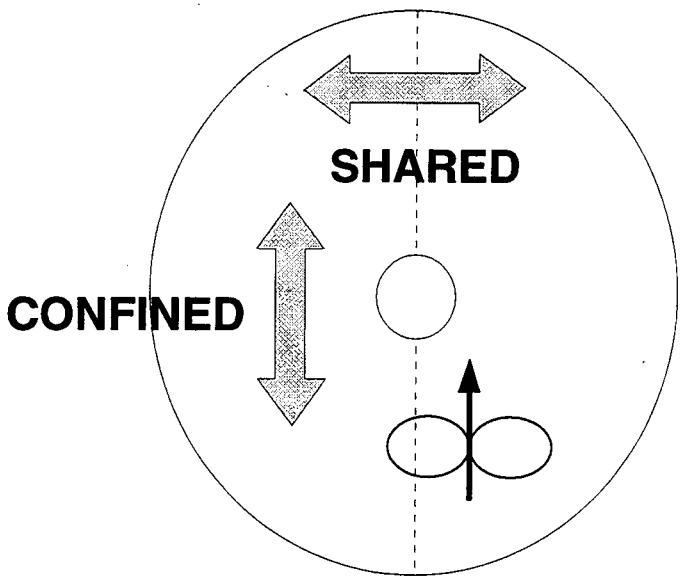

Fig. 4

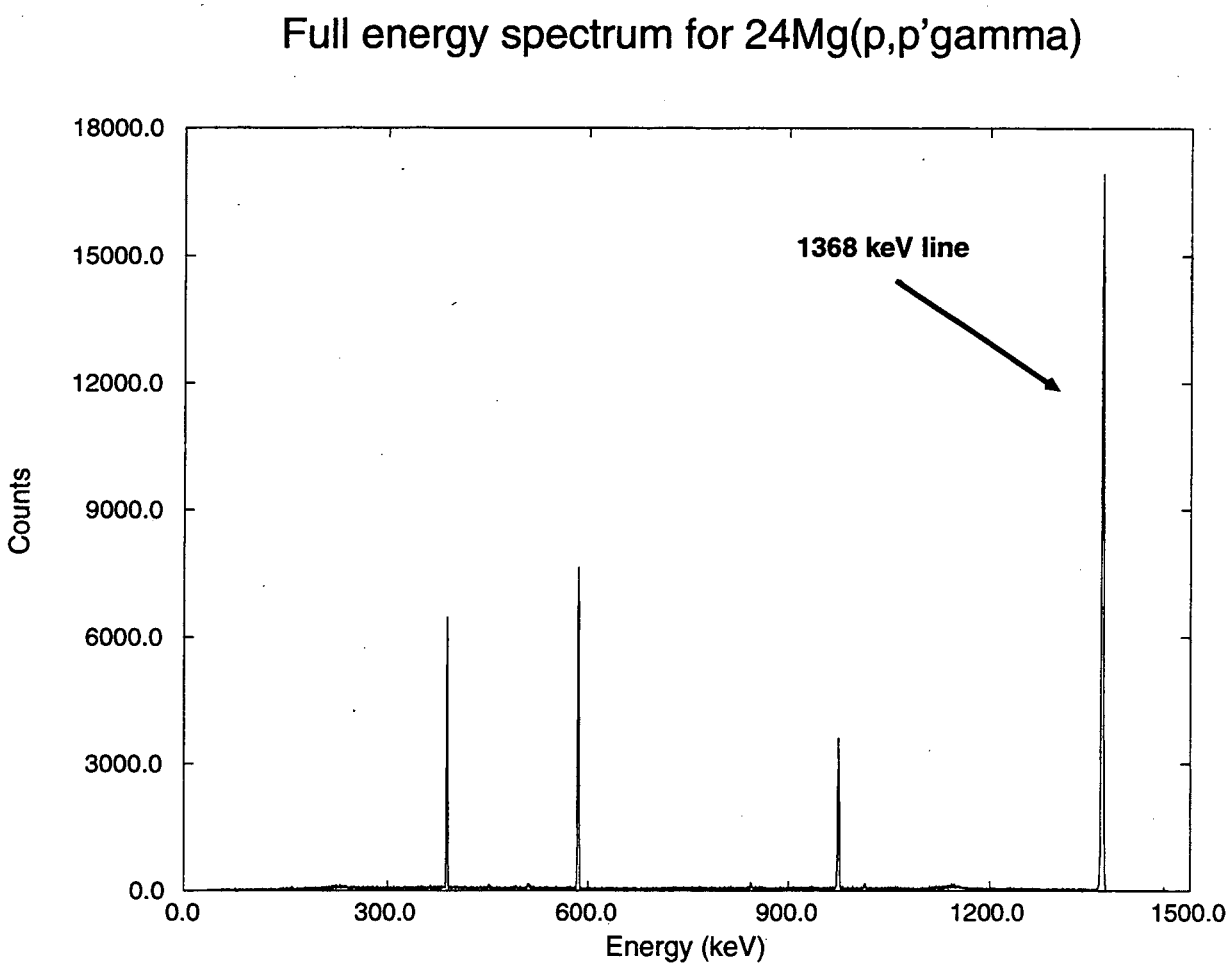
Full energy spectrum for 24Mg(p,p'gamma)
1368 keV line
Counts
Energy (keV)
18000.0
15000.0
12000.0
9000.0
6000.0
3000.0
0.0
0.0
300.0
600.0
900.0
1200.0
1500.0

Fig. 5

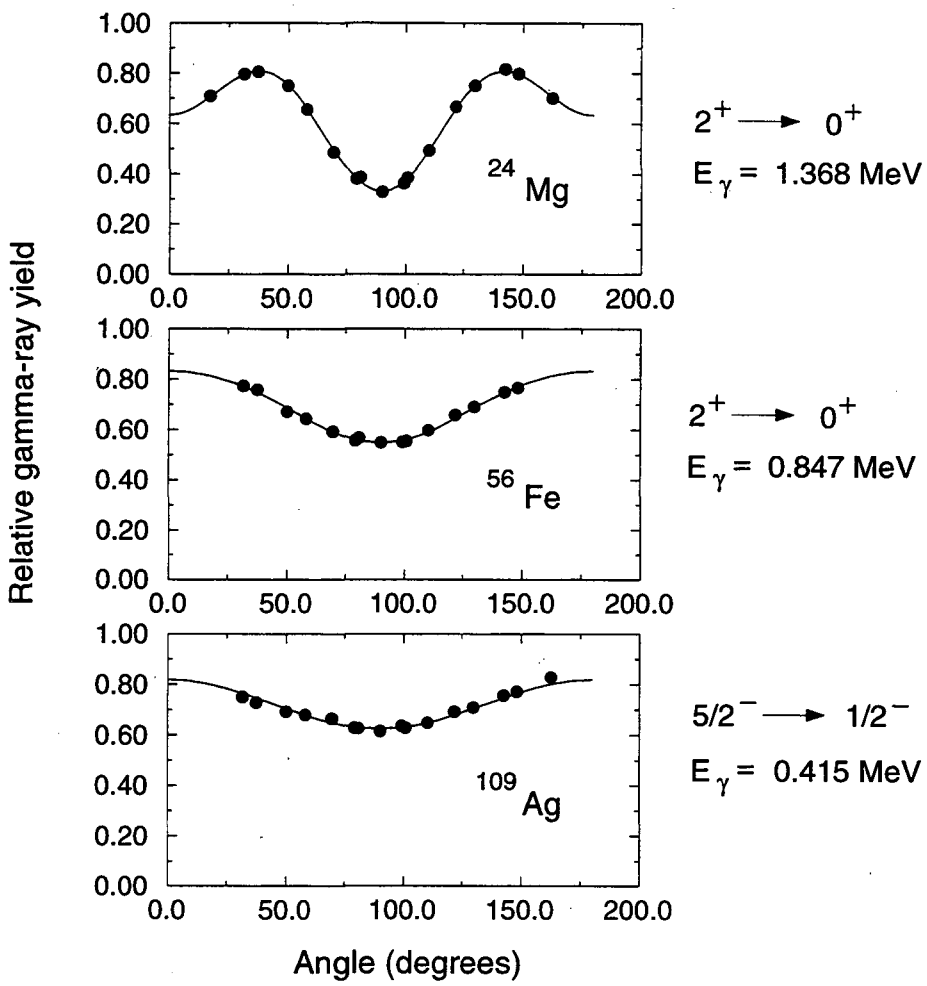
Relative gamma-ray yield
1.00
0.80
0.60
0.40
0.20
0.00
0.0
50.0
100.0
150.0
200.0
24 Mg
2+ → 0+
Eγ = 1.368 MeV
56 Fe
2+ → 0+
Eγ = 0.847 MeV
109 Ag
5/2− → 1/2−
Eγ = 0.415 MeV
Angle (degrees)

Fig. 6

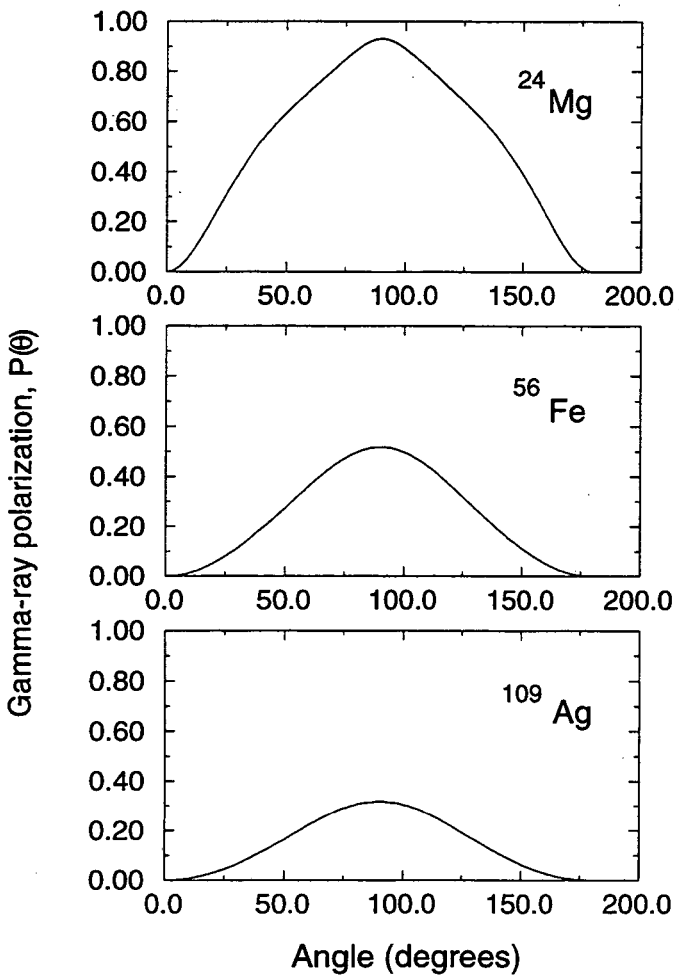
Gamma-ray polarization, P(θ)
1.00
0.80
0.60
0.40
0.20
0.00
0.0
50.0
100.0
150.0
200.0
24Mg
56Fe
109Ag
Angle (degrees)

Fig. 7

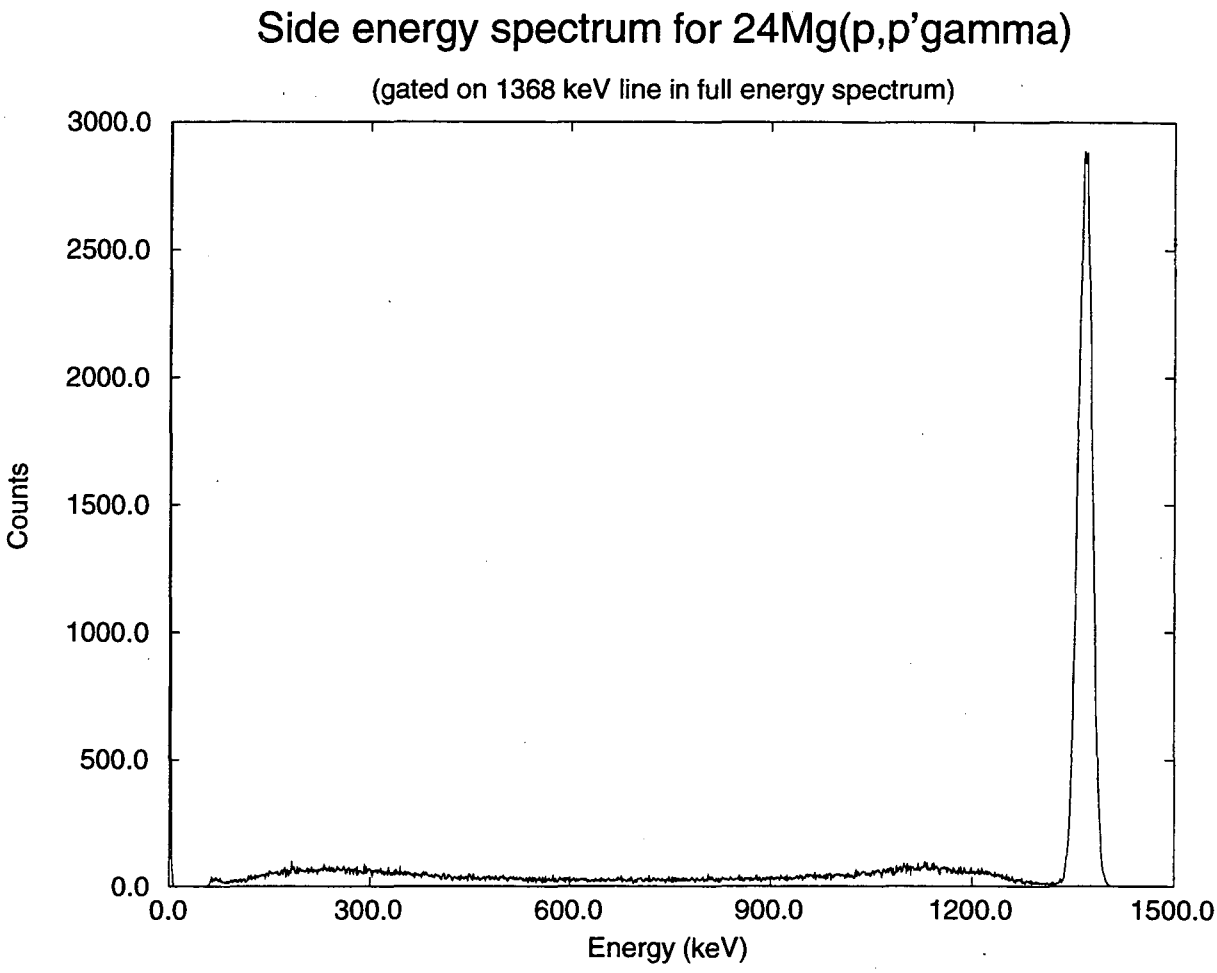
Side energy spectrum for 24Mg(p,p'gamma)
(gated on 1368 keV line in full energy spectrum)
Counts
3000.0
2500.0
2000.0
1500.0
1000.0
500.0
0.0
0.0
300.0
600.0
900.0
1200.0
1500.0
Energy (keV)

Fig. 8

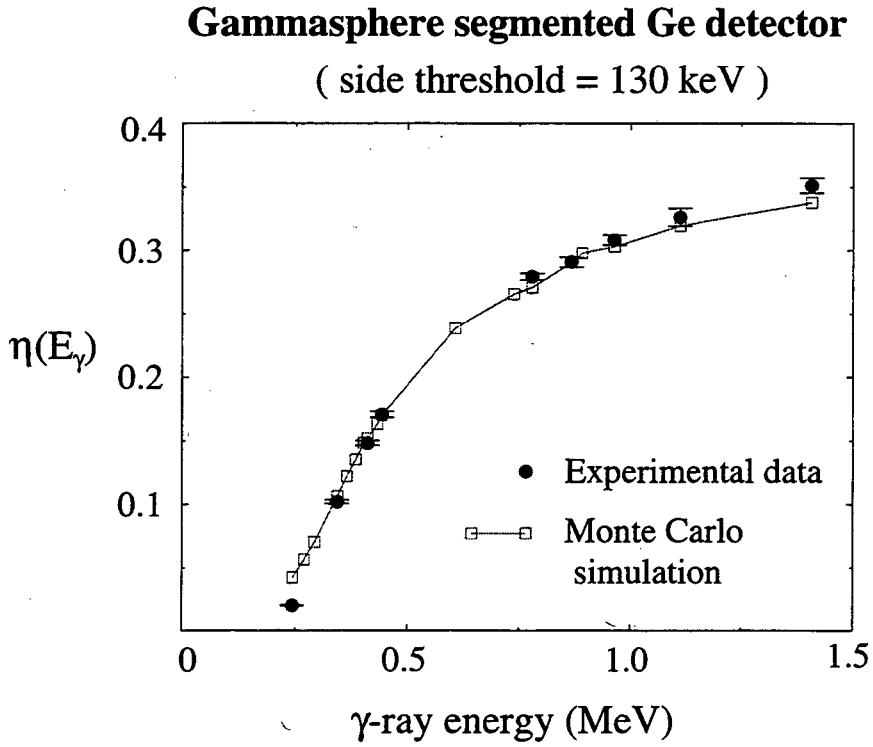
Gammasphere segmented Ge detector
(side threshold = 130 keV)
0.4
0.3
0.2
0.1
η(Eγ)
Experimental data
Monte Carlo simulation
0
0.5
1.0
1.5
γ-ray energy (MeV)

Fig. 9

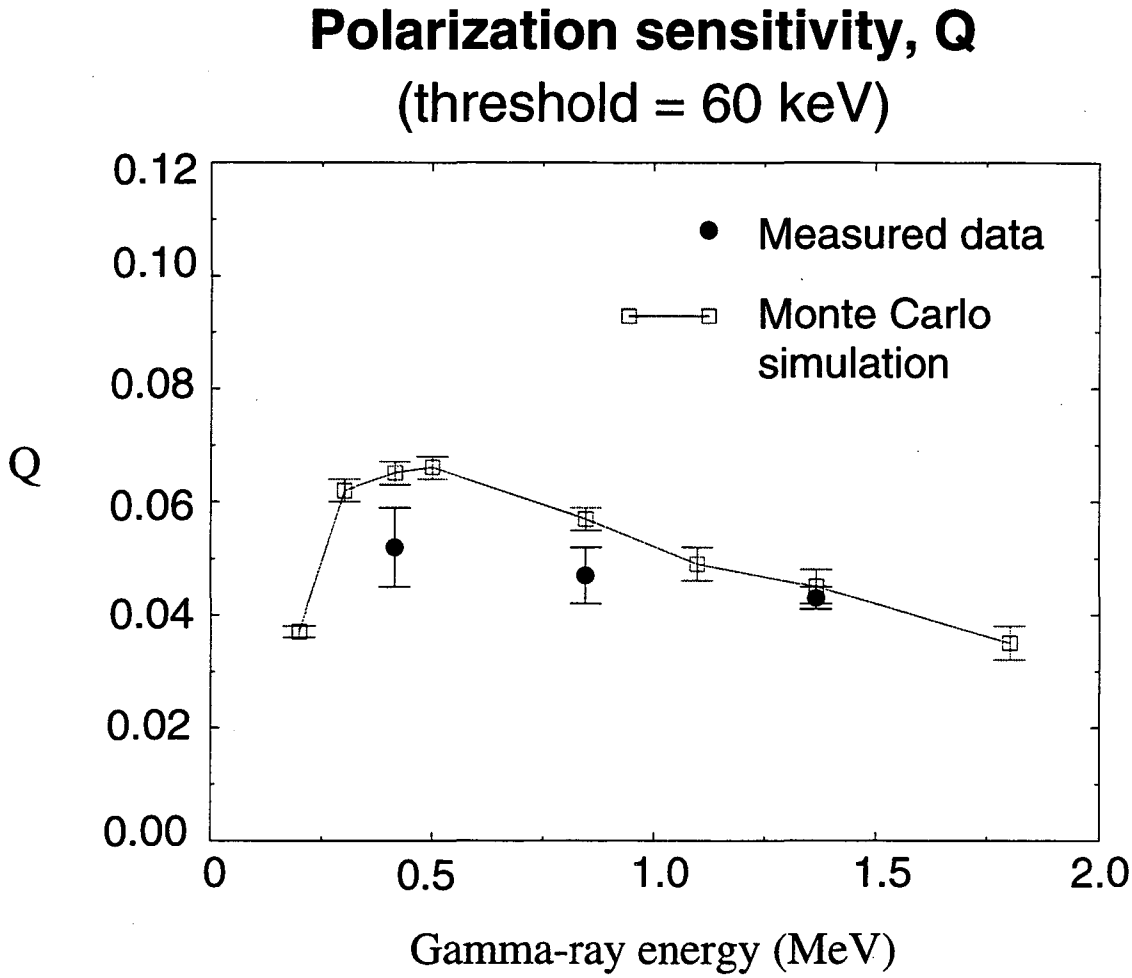
Polarization sensitivity, Q
(threshold = 60 keV)
Measured data
Monte Carlo simulation
Q
0.12
0.10
0.08
0.06
0.04
0.02
0.00
0
0.5
1.0
1.5
2.0
Gamma-ray energy (MeV)

Fig. 10

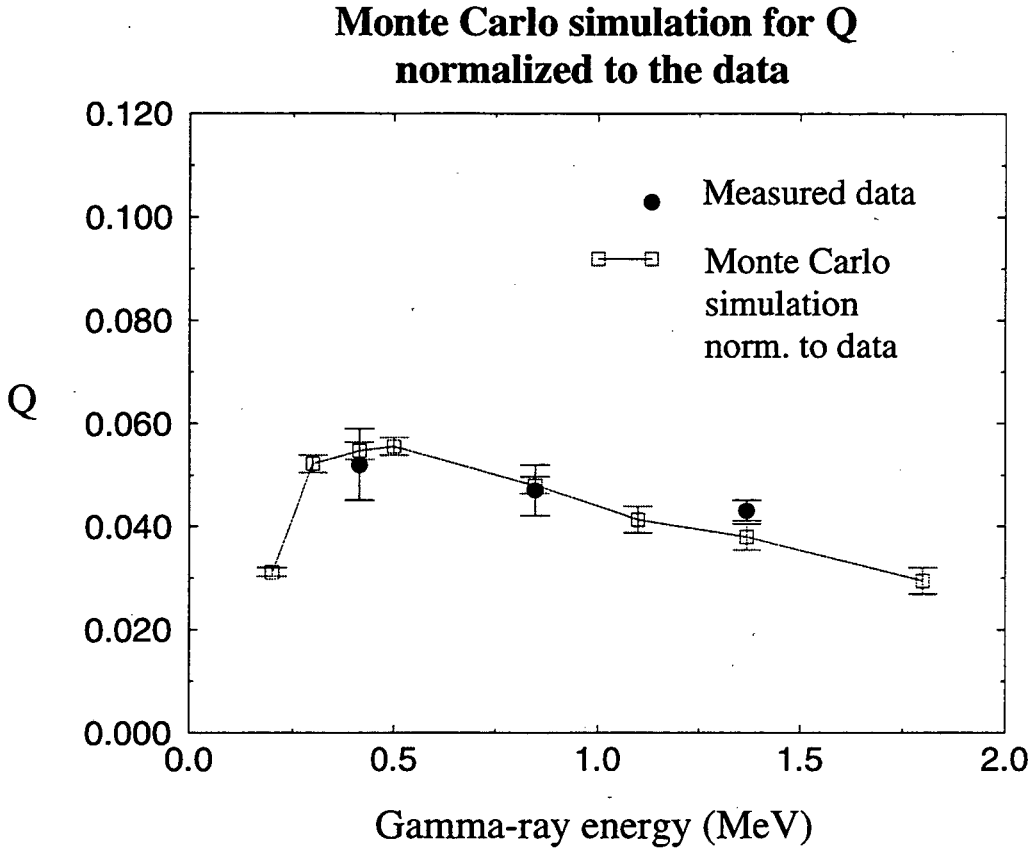
Monte Carlo simulation for Q
normalized to the data
Measured data
Monte Carlo
simulation
norm. to data
Q
0.120
0.100
0.080
0.060
0.040
0.020
0.000
0.0
0.5
1.0
1.5
2.0
Gamma-ray energy (MeV)

Fig. 11

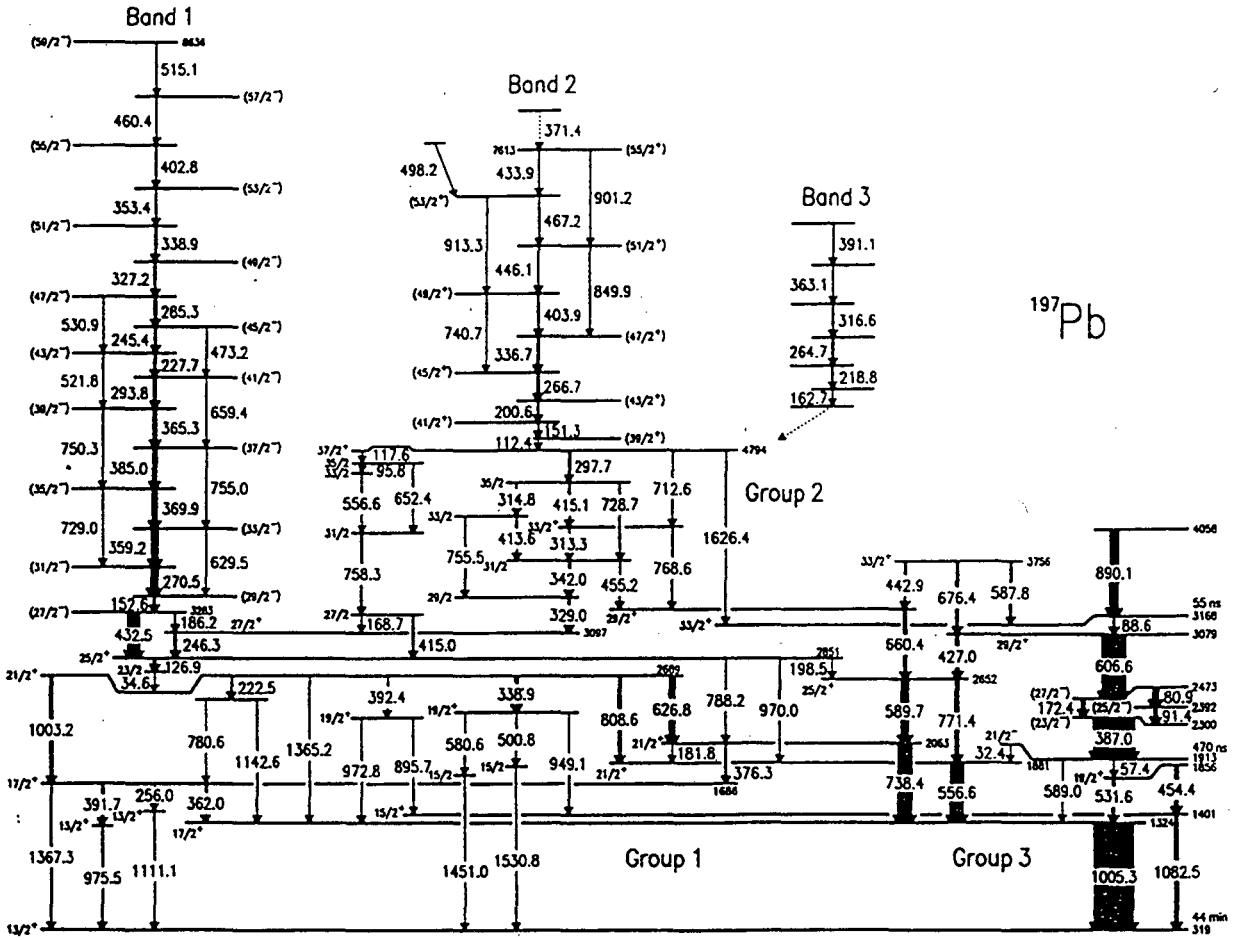
Band 1
Band 2
Band 3
^{197}Pb
Group 1
Group 2
Group 3
515.1
460.4
402.8
353.4
338.9
327.2
285.3
530.9
245.4
227.7
473.2
521.8
293.8
659.4
365.3
750.3
385.0
755.0
369.9
729.0
359.2
629.5
270.5
157.6
186.2
432.5
246.3
126.9
34.6
222.5
1003.2
780.6
1142.6
1365.2
256.0
362.0
391.7
1367.3
975.5
1111.1
371.4
498.2
433.9
901.2
467.2
913.3
446.1
849.9
403.9
740.7
336.7
266.7
200.6
151.3
112.4
117.6
95.8
297.7
556.6
652.4
314.8
415.1
728.7
712.6
413.6
313.3
755.5
342.0
455.2
758.3
768.6
329.0
168.7
415.0
1626.4
392.4
338.9
808.6
626.8
788.2
970.0
198.5
580.6
500.8
949.1
181.8
376.3
972.8
895.7
1451.0
1530.8
391.1
363.1
316.6
264.7
218.8
162.7
442.9
676.4
587.8
660.4
427.0
589.7
771.4
738.4
556.6
890.1
88.6
606.6
80.9
91.4
387.0
57.4
589.0
531.6
454.4
1005.3
1082.5

Fig. 12

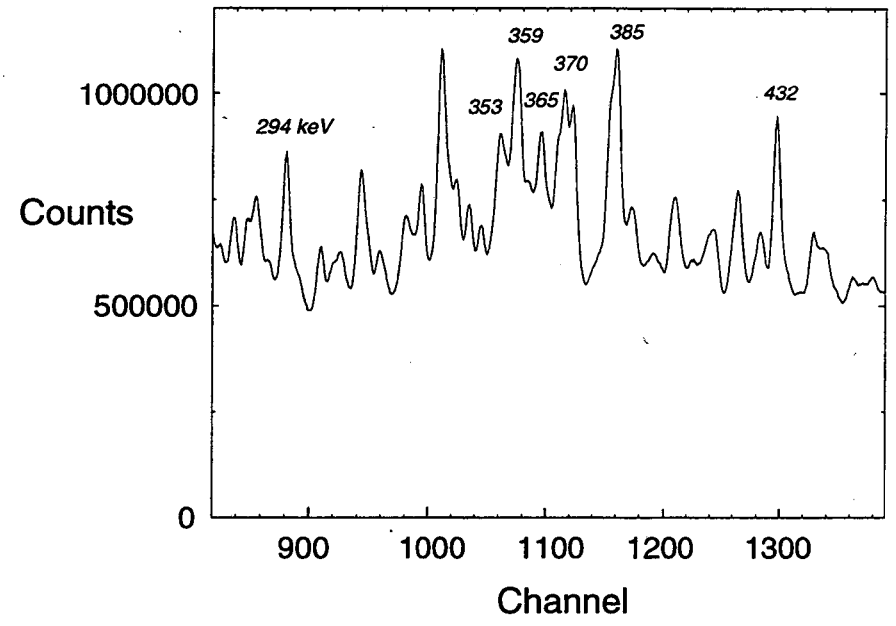

^{197}Pb spectrum:

UNGATED

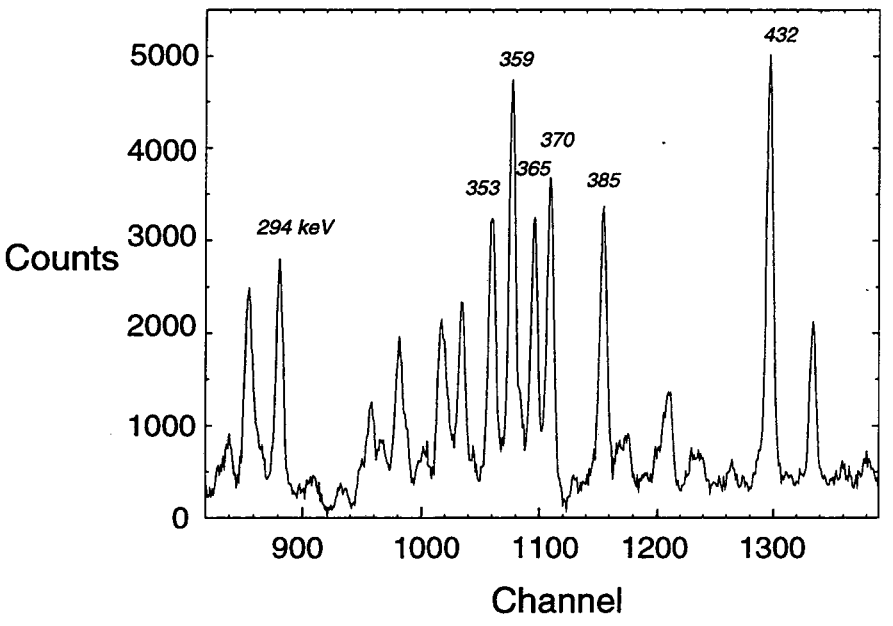

^{197}Pb spectrum:

GATED on 271 keV line
(in-band transition)

Fig. 13

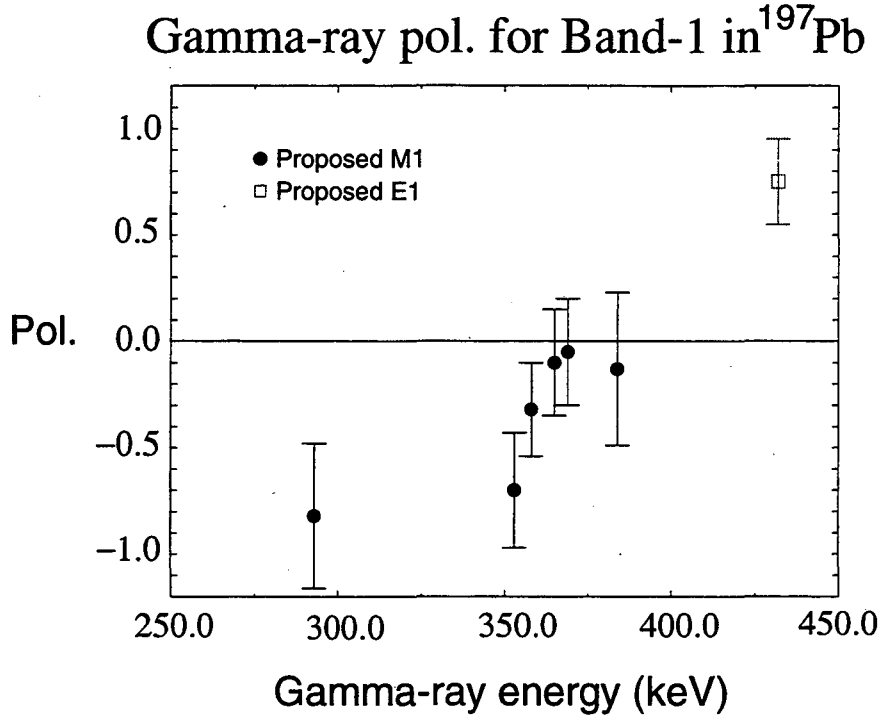
Gamma-ray pol. for Band-1 in ^{197}Pb
Proposed M1
Proposed E1
Pol.
1.0
0.5
0.0
−0.5
−1.0
250.0
300.0
350.0
400.0
450.0
Gamma-ray energy (keV)

Fig. 14

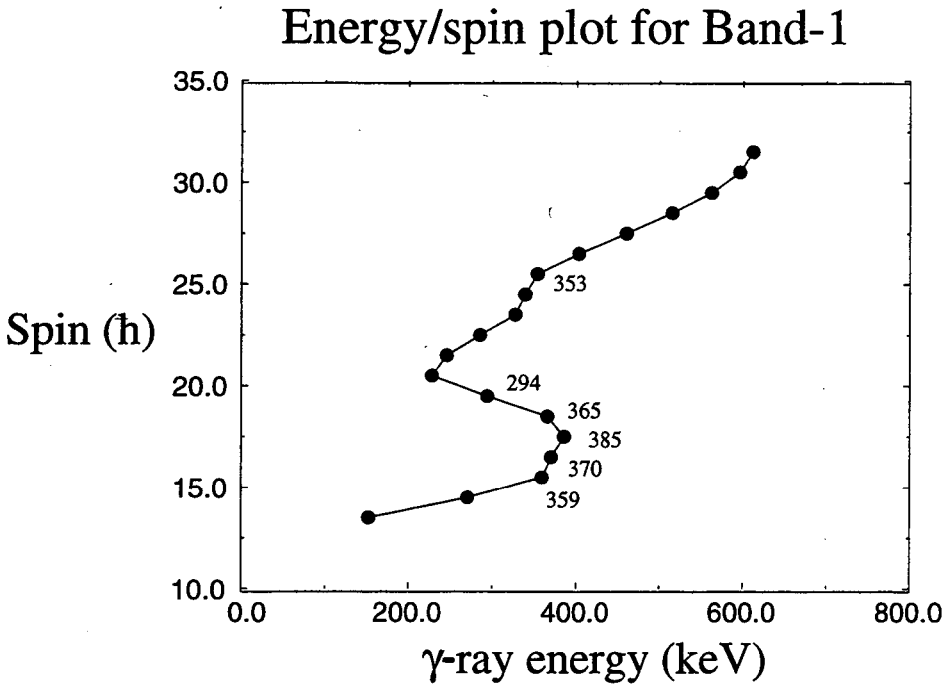
Energy/spin plot for Band-1
Spin (ħ)
35.0
30.0
25.0
20.0
15.0
10.0
0.0
200.0
400.0
600.0
800.0
γ-ray energy (keV)
353
294
365
385
370
359

Fig. 15

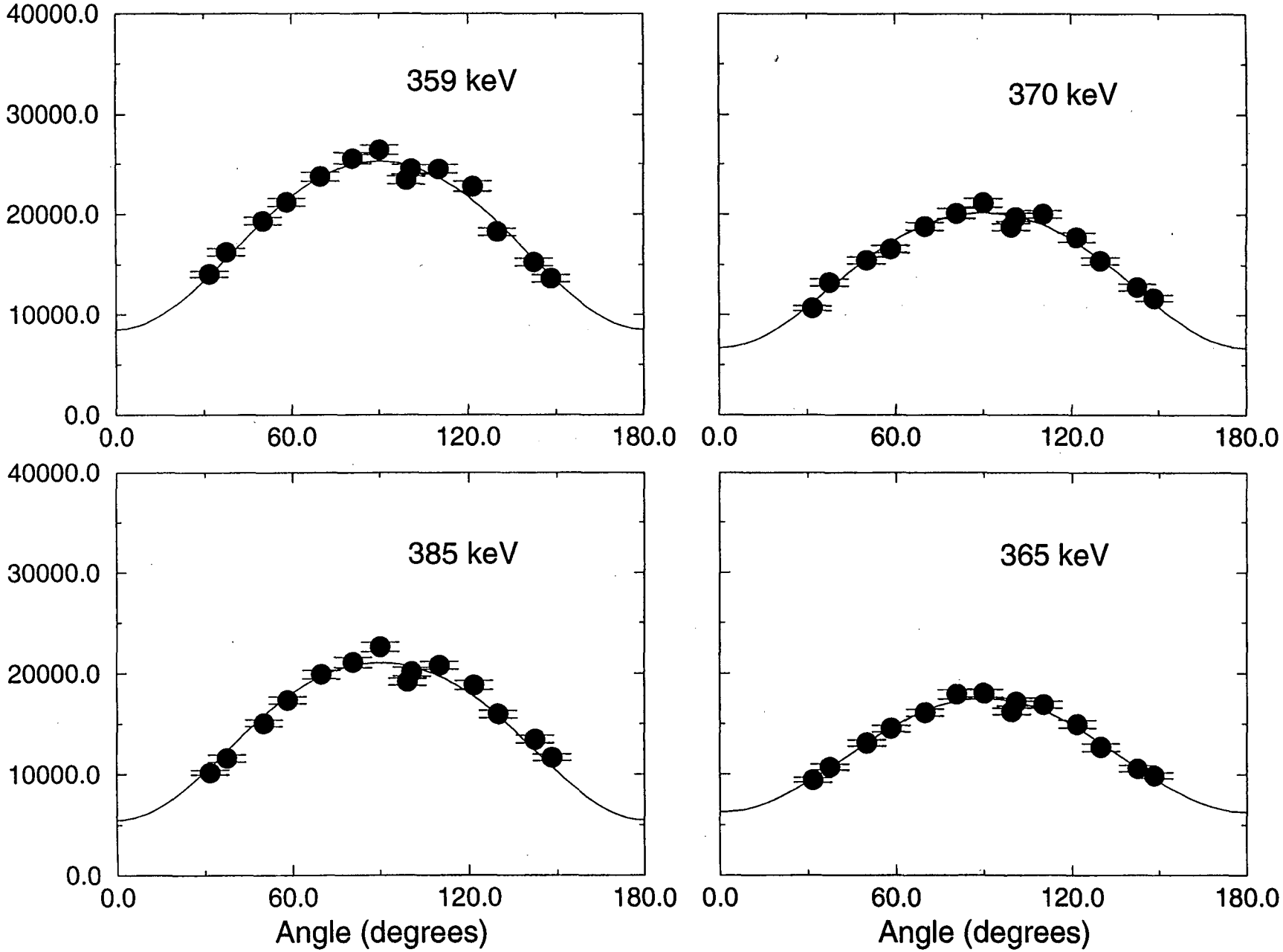
359 keV
370 keV
385 keV
365 keV
40000.0
30000.0
20000.0
10000.0
0.0
0.0
60.0
120.0
180.0
Angle (degrees)

Fig. 16

Ernest Orlando Lawrence Berkeley National Laboratory
One Cyclotron Road | Berkeley, California 94720

Prepared for the U.S. Department of Energy under Contract No. DE-AC03-76SF00098